^{19}F NMR of Trifluoroacetyl-Labeled Cysteine Mutants of Myoglobin: Structural Probes of Nitric Oxide Bound to the H93G Cavity Mutant†

Melissa R. Thomas and Steven G. Boxer*

Department of Chemistry, Stanford University, Stanford, California 94305-5080

Received January 17, 2001; Revised Manuscript Received April 17, 2001

ABSTRACT: Nitric oxide (NO) binds to the myoglobin (Mb) cavity mutant, H93G, forming either a 5- or 6-coordinate Fe−NO heme complex. The H93G mutation replaces the proximal histidine of Mb with glycine, allowing exogenous ligands to occupy the proximal binding site. In the absence of the covalently attached proximal ligand, NO could bind to H93G from the proximal side of the heme rather than the typical diatomic binding pocket on the distal side when the 5-coordinate complex forms. The question of whether NO binds on the distal or proximal side was addressed by ^{19}F NMR. Site-directed mutagenesis was used to introduce unique cysteine residues at the protein surface on either the distal (S58C) or proximal (L149C) side, approximately equidistant from and perpendicular to the heme plane of both wild-type and H93G Mb. The cysteine thiols were alkylated with 3-bromo-1,1,1-trifluoroacetone to attach a trifluoroacetyl group at the mutation site. ^{19}F NMR spectra of 5-coordinate, NO bound S58C/H93G and L149C/H93G double mutants depict peaks with line widths of 100 and 23 Hz, respectively. As fluorine peaks broaden with increasing proximity to paramagnetic centers, such as 5-coordinate Fe−NO, the ^{19}F NMR data are consistent with NO binding in the distal heme pocket of H93G, even in the absence of a sixth axial ligand. Additionally, ^{19}F NMR spectra are reported for deoxy, oxy, CO, met CN, and met H_2O forms of the labeled cysteine mutants. These results demonstrate that the fluorine probes are sensitive to subtle conformational changes in the protein structure due to ligation and oxidation state changes of the heme iron in Mb.

When nitric oxide (NO)[1] binds to heme proteins, it exerts a repulsive *trans*-effect that weakens or breaks the *trans*-axial bond. For example, native myoglobin (Mb) (*1*, *2*) and the *β*-chains of hemoglobin (*3*, *4*) form 6-coordinate NO complexes, where the proximal bond is weakened, but not broken, while the α-chains of hemoglobin (*3*−*5*) and guanylate cyclase (*6*−*9*) form 5-coordinate complexes upon addition of NO. The factors that govern the *trans*-effect, and whether the axial bond ruptures or is only weakened in a particular protein environment, are not clear and are central to understanding how NO exerts its physiological function.

The myoglobin cavity mutant H93G offers an interesting protein-based model system for the systematic investigation of heme−NO complexes. In H93G, the proximal histidine that ligates the iron has been substituted with glycine, generating a cavity adjacent to the iron (*10*). This cavity can be filled with exogenous organic ligands such as imidazole that ligate the iron, thereby mimicking the histidine side chain and restoring properties that are similar, but not identical, to wild-type (WT). In particular, nitric oxide binds wild-type Mb on the distal side of the heme, generating a 6-coordinate complex with NO and the proximal histidine as axial ligands. By contrast, when nitric oxide binds the cavity mutant in the presence of a relatively low concentration of exogenous imidazole (or other organic ligands), the exogenous imidazole−iron bond breaks, and a 5-coordinate complex, denoted H93G-NO, forms (*11*). The coordination states have been characterized in considerable detail by absorption, EPR (*11*), and MCD spectroscopy (*12*, *13*). At high relative imidazole concentration, a 6-coordinate Fe−NO heme complex, referred to as H93G(Im)NO, is formed. Thus, this system has features of both types of NO trans effects. Although it is tempting to assume that NO is in the distal pocket in the H93G-NO 5-coordinate complex, without

† This work is supported in part by Grant GM27738 from the National Institutes of Health to S.G.B. M.R.T. was the recipient of a NSF Predoctoral Fellowship.

* Address correspondence to Steven Boxer at Sboxer@stanford.edu. Phone: (650) 723-4482. Fax: (650) 723-4817.

[1] Abbreviations: NO, nitric oxide; Mb, myoglobin; WT, wild-type; SW, sperm whale; CO, carbon monoxide; MbNO, nitrosylmyoglobin; MbCO, carbonmonoxymyoglobin; MbO_2, oxymyoglobin; metCN Mb, metcyanomyoglobin; met H_2O Mb, Fe(III) Mb with H_2O as an axial ligand; metOH^- Mb, Fe(III) Mb with OH^- as an axial ligand; Im, imidazole; H93G(Im), myoglobin cavity mutant H93G with Im incorporated as an axial ligand; H93G-NO, 5-coordinate complex of NO bound to H93G Mb; H93G(Im)NO, 6-coordinate complex of NO bound to H93G(Im) Mb; S58C, distal cysteine Mb mutant; L149C, proximal cysteine Mb mutant; S58C/H93G, distal cysteine/H93G Mb double mutant; L149C/H93G, proximal cysteine/H93G Mb double mutant; S58C-NO, 6-coordinate NO complex of S58C; L149C-NO, 6-coordinate NO complex of L149C; S58C/H93G-NO, 5-coordinate NO complex of S58C/H93G; L149C/H93G-NO, 5-coordinate NO complex of L149C/H93G; S58C/H93G(Im)NO, 6-coordinate NO complex of S58C/H93G; L149C/H93G(Im)NO, 6-coordinate NO complex of L149C/H93G; TFA, trifluoroacetyl labeling group; GSH, glutathione; GS-TFA, trifluoroacetyl-labeled GSH; NMR, nuclear magnetic resonance; EPR, electron paramagnetic resonance; MCD, magnetic circular dichroism; MALDI-TOF, matrix-assisted laser desorption ionization−time-of-flight mass spectrometry; ESI, electrospray ionization mass spectrometry; PAGE, polyacrylamide gel electrophoresis; ESEEM, electron spin−echo envelope modulation; ENDOR, electron−nuclear double resonance; ESR, electron spin resonance.

10.1021/bi0101087 CCC: $20.00
Published on Web 06/29/2001

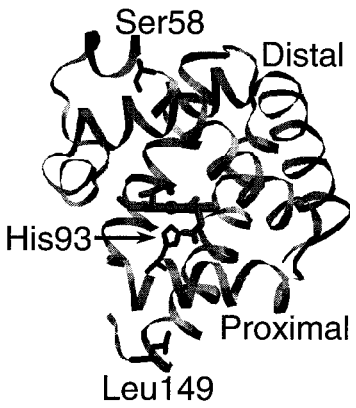

FIGURE 1: Representation of the structure of wild-type sperm whale myoglobin depicting the proximal histidine and sites for cysteine substitution on the distal (Ser58) and proximal (Leu149) sides.

a proximal ligand covalently linked to the protein, it could bind on either the distal side or the proximal side of the heme iron. A related question arises in general for H93G as the distal and proximal pockets are no longer defined by the proximal linkage to the protein backbone. In the case of met H_2O H93G(Im), the X-ray structure unambiguously shows that the exogenous Im is in the proximal cavity (*14*); this has likewise been demonstrated in solution for the met CN and CO forms by extensive proton NMR measurements (*15*, *16*).

To address the question of which side NO binds in H93G-NO, we also looked to NMR techniques for determining local protein structure. Proton NMR data have not been reported for MbNO as NO-bound Mb is a paramagnetic species whose relaxation properties are poorly suited for NMR. Thus, to address the question of the location of NO in H93G-NO, as well as to provide a general method for using NMR to probe Mb samples in all spin and ligation states, we have inserted site-specific probes containing fluorine and monitored their properties by ^{19}F NMR. Fluorine NMR has been used successfully by many research groups to obtain protein structural information. Typically, fluorine is introduced into proteins either through the incorporation of fluorine-substituted amino acids during protein synthesis or by labeling proteins through reaction of a fluorine-containing reagent with specific amino acid groups present in the protein (*17*, *18*). ^{19}F chemical shifts are exquisitely sensitive to structural changes in their local environment, there is no background, and site-specific labeling directly solves the assignment problem (*19*).

We prepared sperm whale Mb mutants in which cysteine is introduced on the proximal and distal surface of the protein in the wild-type and H93G background as shown in Figure 1. (Sperm whale Mb does not contain any cysteine residues.) The cysteine thiol of each mutant was labeled with a trifluoroacetyl (TFA) group by reaction with the reagent 3-bromo-1,1,1-trifluoroacetone (*20*, *21*). Fluorine NMR spectra were obtained for the NO bound forms of each labeled protein. Results of the NMR experiments will be discussed in detail in this paper and are consistent with NO binding on the distal side of the heme in 5-coordinate H93G-NO. Additionally, fluorine NMR spectra are reported for the deoxy, oxy, CO, met CN, and met H_2O forms of the labeled cysteine mutants. Results of these NMR experiments indicate that both the distal and proximal fluorine probes are sensitive to subtle conformational changes in the protein structure due to changes in ligation and oxidation states of the heme iron in Mb.

MATERIALS AND METHODS

Mutagenesis and Protein Preparation. Probe locations were selected on the distal and proximal side of the protein, roughly normal to the heme plane, and approximately equidistant from the heme iron as estimated from wild-type (*22*) and H93G (*14*) crystal structures obtained from the Protein Data Bank (1HJT and 1IRC), respectively. On the basis of these criteria, the mutation sites selected were serine 58 and leucine 149, on the distal and proximal sides, respectively, as shown in Figure 1. The serine 58 O atom is 15.2 Å from the heme iron and lies $\sim -1°$ from normal to the heme plane in the wild-type MbNO crystal structure. The leucine 149 C atom is 15.8 Å from the heme iron and lies $\sim +2°$ from normal to the heme plane in the wild-type crystal structure. These values are taken as the approximate location of the cysteine thiol in the mutant proteins and are of similar magnitude in the H93G(Im) met H_2O crystal structure. Thus, the cysteine residues to which the fluorine probes attach are estimated to be $\sim$15 Å from the heme iron. Wild-type sperm whale Mb was used to create two single amino acid mutants, S58C and L149C. The same mutations were made in the H93G cavity mutant background, creating cysteine/H93G double mutants S58C/H93G and L149C/H93G. Mutagenesis was carried out using the Strategene Quick Change Mutagenesis kit to introduce site-specific mutations in the wild-type Mb plasmid, petMb, and the H93G Mb plasmid, petMb/H93G, isolated from *Escherichia coli* BL21/DE3 cells. Plasmids containing the mutations were transformed and selected by resistance to kanamycin. Successful mutant colonies were selected by sequencing and transformed into BL21/DE3 strain *E. coli* cells for protein expression. *E. coli* BL21/DE3 cell stocks containing the mutant plasmids were grown following previously described procedures (*10*, *15*).

Cell growth was identical for the single and double cysteine mutants with the exception that 10 mM imidazole was added to the culture medium of the double mutants at the time of induction to enhance production and recovery of the cysteine/H93G double mutants. Both single mutants produced dark green colored cells, while the double mutants yielded dark red cell pastes. Protein purification was carried out as previously described (*10*, *15*, *23*) with the exception that the cysteine-containing proteins required reduction with dithiothreitol to eliminate potential disulfide bond formation; 10 mM imidazole was added to all solutions containing the double mutants. Cells were lysed by repeated freeze−thaw and sonication in the presence of lysozyme to free soluble Mb. Cell lysates were dialyzed overnight against 20 mM phosphate buffer, pH 6, containing 1 mM dithiothreitol, followed by dialysis to remove excess dithiothreitol. Protein solutions were purified by ion exchange chromatography using CM-52 carboxymethyl cellulose (Whatman), equilibrated in 20 mM sodium phosphate buffer, pH 6. Each protein was eluted with a NaCl gradient, dialyzed to remove excess salt, concentrated by ultrafiltration, and stored in 50% glycerol solution at -20 °C.

Fluorine Labeling and Characterization. Cysteine thiols were labeled with trifluoroacetyl groups by reaction with

3-bromo-1,1,1-trifluoroacetone (*20*, *21*). Protein stock solutions were dialyzed against 100 mM phosphate buffer, pH 7, to remove glycerol. Solutions were diluted to approximately 100 μM protein concentration and stirred with 3 equiv of 3-bromo-1,1,1-trifluoroacetone at room temperature for 30 min. Excess labeling reagent was removed by gel-filtration with Sephadex G25 chromatography resin (Pharmacia). Protein fractions were concentrated by diafiltration using centricons (Amicon/Millipore) and stored briefly at 4 °C until used. The extent of labeling was assessed spectrophotometrically by detection of free thiols with Ellman's reagent, [5,5′-dithiobis(2-nitrobenzoic acid)] (*24*). Reaction conditions were 100 μM Ellman's reagent, 2 μM protein, 100 mM phosphate buffer, pH 7, monitored at 412 nm. MALDI-TOF and electrospray ionization (ESI) mass spectrometry were also used to confirm that the cysteine thiols were successfully labeled with the trifluoroacetyl group.

Preparation of Protein NMR Samples. Fluorine NMR samples were prepared by diluting concentrated solutions of trifluoroacetyl (TFA)-labeled cysteine mutants with 100 mM phosphate buffer containing 15% D_2O, pH 7 (pH uncorrected for deuterium). Solutions of the double mutants also contained 10 mM imidazole. Final concentrations of NMR samples ranged from 0.1 to 3 mM Mb. Prior to dilution, concentrated protein solutions were prepared with the appropriate diatomic ligand. Deoxy Mb samples were prepared by purging concentrated protein samples with N_2 for 1 h, followed by reduction with 1−2 equiv of freshly prepared 1 M solutions of sodium dithionite (Fluka). Carbonmonoxy Mb samples were prepared similarly with the additional step of purging the reduced sample with CO gas (Matheson) for 30 min. For oxy Mb samples, dithionite-reduced protein solutions were exposed to air. Ferrous NO samples were prepared by purging reduced protein samples with 100% NO gas (Matheson) for 5 min before diluting with buffer. Ferrous 5-coordinate NO samples of the double mutants were prepared by removal of imidazole by diafiltration, followed by reduction with dithionite and addition of NO gas in the absence of O_2. Ferric protein samples were prepared by the addition of oxidizing agents to concentrated protein stocks. Met CN samples were prepared by adding 10 mM potassium cyanide to the protein solution. Met H_2O samples were prepared either by allowing MbO_2 samples to autooxidize or by addition of a slight excess of freshly prepared potassium ferricyanide to oxidize the sample, followed by removal of excess potassium ferricyanide by gel filtration. In each case, results obtained for met H_2O samples prepared by chemical oxidation and autoxidation were identical.

Air-sensitive samples were transferred via gastight syringe to 5 mm NMR tubes that had been sealed with rubber septa and purged with N_2 gas. Data were collected for samples prepared individually as described above. Additionally, data were collected for each protein sample cycled through as many ligation states as possible. For example, spectra were collected for the same sample prepared first as the deoxy form, followed by purging with CO gas to generate MbCO, and then CO was replaced with NO gas to form MbNO. Likewise, spectra were collected for a second sample prepared first as deoxy Mb, purged with O_2 to generate MbO_2, followed by allowing autoxidation to form met H_2O Mb, and finally addition of 10 mM potassium cyanide to form MbCN. In each case, the data were identical for samples prepared individually as compared with those cycled through several ligation states. Furthermore, after collecting spectra for each 5-coordinate MbNO sample, imidazole was reintroduced to the sample (to a final concentration of 10 mM imidazole) to form the corresponding 6-coordinate MbNO species. Spectra obtained for the 6-coordinate species prepared in this manner were identical to spectra obtained for the 6-coordinate double mutant MbNO samples prepared independently of the 5-coordinate species.

UV/Vis Spectroscopy. A Perkin-Elmer Lambda 12 UV/vis spectrometer was used to acquire electronic absorption spectra of all samples preceding and following NMR spectroscopy to verify the heme iron ligation state. UV/vis spectra were measured in sealed, anaerobic, quartz cuvettes (1-cm path length) containing 1−2 μM protein, 100 mM phosphate buffer, pH 7, and 10 mM imidazole for the H93G double mutants. Spectra of concentrated NMR samples were also measured using a sample cell constructed of glass slides separated by a 75 μM Mylar spacer to avoid dilution effects.

NMR Spectroscopy. Fluorine NMR spectra were collected at 470 MHz using a GE Omega NMR spectrometer equipped with a proton probe modified for ^{19}F (Fremont Magnetic Resonance, Fremont, CA). Chemical shift values were referenced to 5 mM trifluoroacetic acid as an external standard. Typical single pulse experiments consisted of a 58 μs pulse width and a pre-delay of 2 s. Temperature dependence measurements were collected in intervals of 5 °C from 5 °C to 40 °C. Data were apodized by an exponential function with a line broadening factor of 3 Hz, except for spectra used for the line width analysis. T_1 values were determined by standard $180°-\tau-90°$ inversion recovery experiments. One-dimensional ^1H NMR spectra were acquired for the met CN and CO bound forms of the proteins to determine the effect of mutation on the heme environment of wild-type and H93G Mb as previously described (*15*, *16*).

RESULTS

Protein Characterization. Cysteine mutant proteins were isolated and purified as described above, producing approximately 250 mg of protein per 12 L of fermentation culture. SDS−PAGE of each purified protein demonstrated isolation of purified, monomeric protein, while nondenaturing PAGE confirmed the formation of folded Mb with no evidence of disulfide bond formation. Electronic absorption spectra of S58C, L149C, S58C/H93G, and L149C/H93G samples with a variety of distal ligands closely resemble wild-type and H93G(Im) spectra. Characteristic values for the absorption maxima of spectra for each ligation state are available in the Supporting Information.

Efficiency of the Thiol Labeling Reaction. The extent of cysteine thiol labeling was determined by reaction of unlabeled thiols with Ellman's reagent. Changes in UV/vis absorption, monitored at 412 nm, indicate that greater than 95% of the cysteine thiols are labeled in each of the samples. MALDI-TOF and ESI mass spectrometry were also performed for both labeled and unlabeled samples of each variant. Masses obtained for the unlabeled proteins agree with values calculated for the apoprotein sequences, accounting for natural isotope abundance. M/Z peaks measured for the labeled proteins were found to be 111 amu greater than that

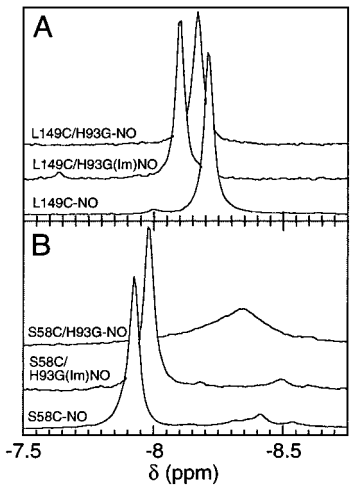

FIGURE 2: ^{19}F NMR spectra for NO bound forms of the TFA-labeled proximal and distal cysteine mutants. (A) Proximal mutants: 6-coordinate L149C-NO, 6-coordinate L149C/H93G(Im)-NO, and 5-coordinate L149C/H93G-NO. (B) Distal mutants: 6-coordinate S58C-NO, 6-coordinate S58C/H93G(Im)NO, and 5-coordinate S58C/H93G-NO. Protein concentrations were 1−3 mM in 100 mM phosphate buffer, pH 7, 15% D_2O. Six-coordinate L149C/H93G(Im)NO and S58C/H93G(Im)NO protein solutions also contained 10 mM imidazole. All spectra were collected as 2048 scans of 2 K points with a spectral window of 7168.5 Hz, and chemical shifts are referenced to an external standard of 5 mM trifluoroacetic acid.

for the corresponding unlabeled proteins, a mass difference that is consistent with the attachment of a single -CH_2−CO−CF_3 unit at the cysteine thiol for each labeled protein.

^{19}F NMR of NO-Bound, Trifluoroacetyl-Labeled Cysteine Mutants. Fluorine NMR spectra of TFA-labeled L149C-NO, L149C/H93G(Im)NO, and 5-coordinate L149C/H93G-NO are shown in Figure 2, panel A. Fluorine NMR spectra of TFA-labeled S58C-NO, S58C/H93G(Im)NO, and 5-coordinate S58C/H93G-NO are shown in Figure 2, panel B. The corresponding chemical shifts and temperature dependence data for each protein are listed in Table 1. For ease of comparison, line width values and the corresponding experimental error are listed in Table 2. In general, the chemical shift values of the 6-coordinate single and 6-coordinate double mutants are quite similar. Fluorine peaks in the spectra for L149C-NO and L149C/H93G(Im)NO exhibit similar chemical shifts and line widths, and the fluorine signal for S58C-NO is quite similar in chemical shift and line width to that of S58C/H93G(Im)NO. However, chemical shifts differ between the distal and proximal mutants due to intrinsic differences in the local environment of the fluorine nuclei at the two cysteine labeling sites. More significantly, the line width for each ligation state of both single and double Mb mutants is broader for the distal side (S58C) than for the proximal side mutant (L149C), see Table 2. Comparison of spectra for the 6- and 5-coordinate NO complexes of the L149C/H93G double mutant reveals similar chemical shift values, although the line width broadens by ∼6 Hz for the 5-coordinate proximal mutant. In contrast, spectra of the 6- and 5-coordinate NO complexes of the S58C/H93G double mutant exhibit significant differences in chemical shift and line width. The 5-coordinate, distal, double mutant peak shifts upfield by 0.4 ppm and broadens by ∼80 Hz relative to the 6-coordinate S58C/H93G(Im)NO sample.

^{19}F NMR of Various Ligation States of Trifluoroacetyl-Labeled Cysteine Mutants. Fluorine NMR spectra of deoxy, CO, NO, oxy, met H_2O, and met CN bound forms of TFA-labeled L149C, L149C/H93G(Im), S58C, and S58C/H93G(Im) are shown in Figure 3. Chemical shift and temperature dependence data are listed in Table 1. All chemical shift values are reported relative to an external standard of 5 mM trifluoroacetic acid. Line width values and the corresponding experimental error for each spectrum are listed in Table 2. The spectra exhibit a total chemical shift range of 1.3 ppm. In general, the chemical shift values of the met CN adduct of the labeled cysteine proteins fall in the range of −7.46 to −7.63 ppm, while all chemical shift values for met H_2O samples range between −8.14 and −8.75 ppm. Overall, the pattern of chemical shift values for deoxy/oxy, CO, and NO differ for the two sides of the protein: CO > NO > deoxy ≈ oxy for the distal side mutants, and deoxy ≈ oxy > CO > NO for the proximal side mutants (downfield to upfield). Deoxy and oxy chemical shift values of each mutant are quite similar, although they span the range of −7.85 to −8.42 ppm for all four mutants together. Double mutant peaks for deoxy samples are shifted downfield relative to their corresponding single mutants by 0.10 and 0.04 ppm for L149C and S58C,

Table 1: ^{19}Fluorine NMR Data for TFA-Labeled Cysteine Mb Variants

	chemical shift (ppm)[a] [temp. shift (× 10^2) (ppm/°C)]					
protein	deoxy	CO	NO	oxy	met H_2O	met CN
S58C	−8.42 [0.69]	−7.88 [0.12]	−7.94	−8.39	−8.14	−7.63
L149C	−7.98 [−0.16]	−8.21 [−0.27]	−8.20	−8.00 [−0.16]	−8.75 −8.21	−7.56 [−0.50]
S58C/H93G(Im)[c]	−8.38 [0.75]	−7.94	−7.98 [0.22]	−8.37	−8.19	−7.61
L149C/H93G(Im)[b,c]	−7.85 [−0.15]	−8.10 [−0.20]	−8.11 [−0.24]	−7.87 [−0.22]	−7.64 [−0.33] −8.63	−7.46 [−0.56]
S58C/H93G-NO[d]			−8.38 [0.82]			
L149C/H93G-NO[d]			−8.18 [−0.17]			

[a] Chemical shifts are referenced to 5 mM trifluoroacetic acid external standard. The experimental error observed for chemical shift values was typically ± 0.02 ppm. [b] The CO and oxy forms of L149C/H93G(Im) were also prepared using hexaammineruthenium(III) chloride (2−4 equiv) as a reducing agent. Solutions of 50 mM hexaammineruthenium(III) chloride were prepared in 20 mM Tris buffer, pH 7, by degassing with N_2 sparge over mossy zinc. The ruthenium solution was diluted into NMR samples, substituting for sodium dithionite in the sample preparation methods described above. Samples prepared using this alternative reducing agent generated NMR and electronic absorption spectra that were identical to samples prepared with low concentrations (1−3 equiv) of sodium dithionite as a reducing agent. [c] S58C/H93G(Im) and L149C/H93G(Im) refer to the 6-coordinate distal/H93G and 6-coordinate proximal/H93G double mutants with imidazole bound. [d] S58C/H93G-NO and L149C/H93G-NO refer to the 5-coordinate MbNO complexes of the distal/H93G and proximal/H93G double mutants. The 5-coordinate double mutant complexes are only observed for the MbNO ligation state.

Table 2: ^{19}Fluorine NMR Linewidths for TFA-Labeled Cysteine Mb Variants[a]

protein	deoxy	CO	NO	oxy	met H_2O	met CN
S58C	24 ± 0.6	18 ± 1	19 ± 0.6	20 ± 1	23 ± 0.6	18 ± 0.5
L149C	17 ± 0.7	15 ± 0.8	17 ± 0.7	16 ± 1	16, 17 ± 0.5	15 ± 0.3
S58C/H93G(Im)[b]	22 ± 1	16 ± 0.5	18 ± 0.8	19 ± 1	17 ± 0.6	16 ± 0.5
L149C/H93G(Im)[b]	16 ± 0.7	15 ± 1	17 ± 0.8	14 ± 0.7	12, 14 ± 0.4	15 ± 0.7
S58C/H93G-NO[c]			100 ± 10			
L149C/H93G-NO[c]			23 ± 2			

[a] Line widths were determined from spectra that were transformed without apodization to avoid line broadening. Error values indicated in the table are the standard deviation of line width values that were obtained for 3−5 different sample preparations of each ligation state. [b] S58C/H93G(Im) and L149C/H93G(Im) refer to the 6-coordinate distal/H93G and 6-coordinate proximal/H93G double mutants with imidazole bound. [c] S58C/H93G-NO and L149C/H93G-NO refer to the 5-coordinate MbNO complexes of the distal/H93G and proximal/H93G double mutants. The 5-coordinate double mutant complexes are only observed for the MbNO ligation state.

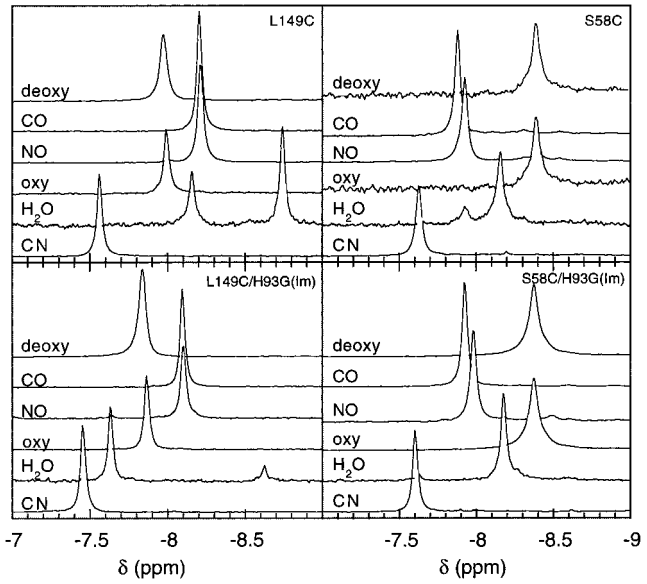

FIGURE 3: ^{19}F NMR spectra for deoxy, CO, NO, oxy, met H_2O, and met CN bound forms of TFA-labeled proximal and distal cysteine mutants. (Upper left panel): proximal single mutant, L149C; (lower left panel): proximal double mutant, L149C/H93G-(Im); (upper right panel): distal single mutant, S58C; (lower right panel): distal double mutant, S58C/H93G(Im). All spectra were collected as 2048 scans of 2 K points with a spectral window of 7168.5 Hz, and chemical shifts are referenced to an external standard of 5 mM trifluoroacetic acid.

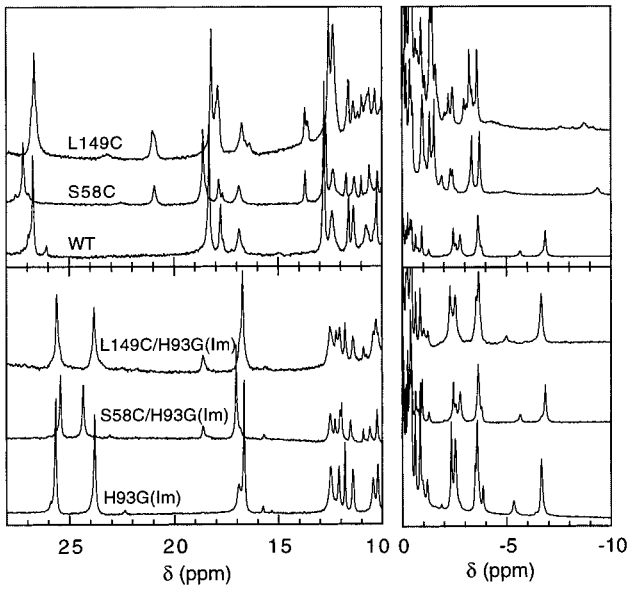

FIGURE 4: ^{1}H NMR spectra for the met CN bound form of TFA-labeled, proximal and distal cysteine mutants. (Upper panels) Proximal single mutant L149C, distal single mutant S58C, and wild-type. (Lower panels) Proximal double mutant L149C/H93G(Im), distal single mutant S58C/H93G(Im), and H93G(Im). All spectra were collected as 512 scans of 8 K points with a spectral window of 25 000 Hz.

respectively. CO bound distal mutants exhibit peaks that shift downfield by approximately 0.58 ppm relative to the deoxy form. In contrast, the CO form of the proximal mutants shifts upfield by 0.25 ppm relative to the deoxy form. CO and 6-coordinate NO chemical shift values are identical for L149C as well as for L149C/H93G, while CO and 6-coordinate NO chemical shift values differ by 0.06 and 0.05 ppm for S58C and S58C/H93G, respectively. Chemical shifts for the 6-coordinate NO samples differ for the double and single mutants: the distal double mutant is 0.05 ppm upfield of the distal single mutant, while the proximal double mutant falls 0.11 ppm upfield of the proximal single mutant. The chemical shift of the 5-coordinate NO form of S58C/H93G is identical to the chemical shift of the deoxy or oxy form of S58C/H93G and falls 0.4 ppm upfield of the 6-coordinate NO form. In contrast, the chemical shift value for 5-coordinate L149C/H93G-NO is similar to that of 6-coordinate L149C/H93G(Im)NO but is observed 0.33 ppm upfield of the deoxy or oxy form of L149C/H93G.

Temperature dependence data for the ^{19}F NMR spectra of each mutant in various ligation states are presented in brackets in Table 1. Changes in chemical shifts as a function of temperature were determined relative to an external standard of 5 mM trifluoroacetic acid. Changes in chemical shift values for the fluorine-labeled Mb mutants range from −0.0056 to +0.0082 ppm/°C. Spectra of the proximal cysteine mutants L149C and L149C/H93G exhibit decreasing chemical shift values with increasing temperature (anti-Curie behavior). In contrast, spectra of the distal mutants obey Curie behavior, with chemical shift values shifting downfield with temperature.

T_1 relaxation times were measured for L149C-CO, L149C-NO, S58C-NO, L149C/H93G(Im)CO, oxy L149C/H93G-(Im), and met H_2O L149C/H93G(Im) and are 343, 336, 360, 352, 321, and 370 ms, respectively. The T_1 values for the protein samples are similar, while T_1 values for 3-bromo-1,1,1-trifluoroacetone and TFA-labeled glutathione are 1.5 s and 590 ms, respectively.

^{1}H NMR Spectra of Met CN and CO Bound Cysteine Mutants. Proton NMR spectra of met CN bound wild-type, L149C, and S58C in the hyperfine-shifted region are shown in Figure 4, upper panels. Proton NMR spectra of met CN bound H93G, L149C/H93G(Im), and S58C/H93G(Im) are shown in Figure 4, lower panels. Although individual

resonances have not been assigned explicitly, the general appearance of the spectra is quite similar to that of the wild-type or H93G(Im) spectra in the case of the single and double mutants, respectively. Hyperfine-shifted peaks are quite different between wild-type and H93G(Im) because of the orientation of the exogenous imidazole (*15*). Chemical shift values for the heme methyl and Ile99 marker peaks that are sensitive to the heme pocket geometry are listed in Tables 2 and 3 of the Supporting Information for met CN and CO bound samples, respectively. Proton NMR spectra of met CN and CO bound samples of single mutants are not significantly different from the met CN and CO spectra of wild-type Mb (*25*−*27*). Likewise, proton NMR spectra of met CN and CO bound samples of double mutants are not significantly different from the met CN and CO spectra of H93G(Im) (*15, 16*). Chemical shift values for the mutants typically vary by less than 0.2 ppm, on average, as compared to corresponding peaks in the wild-type or H93G met CN and CO reference spectra. The nominal apparent differences between the mutant and wild-type reference spectra suggest that introduction of the cysteine residues at L149 and S58 minimally perturbs the tertiary structure of the proteins in the vicinity of the heme.

Effect of Sodium Dithionite on Trifluoroacetyl-Labeled Glutathione. In the course of these studies, we noticed that treatment of the TFA-labeled protein samples with a large excess of sodium dithionite during the preparation of deoxy, CO, or NO samples caused the ^{19}F NMR signal to shift downfield by 11 to 12 ppm. To examine this observation, we performed a series of control experiments in which the cysteine thiol of glutathione was labeled with 3-bromo-1,1,1-trifluoroacetone as described for the protein samples. TFA-labeled glutathione samples were column purified, lyophilized, and dissolved in 100% D_2O equilibrated with N_2 gas for ^{19}F and ^{1}H NMR spectroscopy in sealed NMR tubes. Following NMR spectroscopy, TFA-labeled glutathione samples were injected with 5 to 10 equiv of freshly prepared sodium dithionite, and NMR spectroscopy was repeated to determine the effect of dithionite on labeled cysteine residues.

Proton NMR spectra of glutathione, trifluoroacetyl-labeled glutathione (GS-TFA), and GS-TFA treated with dithionite are shown in the upper panel of Figure 1 in the Supporting Information. The proton spectrum of GS-TFA clearly depicts chemical shifts and proton splitting patterns characteristic of an alkylated cysteine thiol (*28*). Addition of dithionite to labeled glutathione induces a slight broadening of some peak line widths and causes significant changes in the splitting pattern and chemical shift of the multiplet located at 3.0 ppm. The resulting spectrum is quite similar to published spectra of TFA-labeled glutathione following reaction with the reducing agent, sodium borohydride (*28*). Comparison of observed and published spectra shows the data to be consistent with sodium dithionite reducing the ketone of the TFA labeling group to an alcohol.

Further evidence of the chemical modification of the trifluoroacetyl moiety by sodium dithionite is observed in the ^{19}F NMR spectra of TFA-labeled glutathione before and after reaction with sodium dithionite, as shown in the lower panel of Figure 1 in the Supporting Information. Exposure to sodium dithionite causes the ^{19}F resonance of TFA-labeled glutathione to shift downfield from −9.28 ppm and split into two peaks at 2.97 and 3.02 ppm. The resulting ^{19}F NMR spectrum is consistent with the published ^{19}F NMR spectrum of sodium borohydride reduced, TFA-labeled glutathione (*28*). Both ^{1}H and ^{19}F NMR data indicate that sodium dithionite reduces the ketone of the trifluoroacetyl labeling group to an alcohol, generating the two epimers corresponding to two peaks in the ^{19}F NMR spectrum.

The results obtained from glutathione control experiments explain the observed effect of a large excess of sodium dithionite on the trifluoroacetyl-labeled Mb cysteine mutants. To avoid deleterious effects of sodium dithionite, we used only a slight excess of sodium dithionite (1−3 equiv) to reduce heme in the labeled Mb samples. Alternatively, milder reducing agents such as hexaammineruthenium(III) chloride can be used without affecting the fluorine labeling group, while still achieving reduction of the heme iron.

DISCUSSION

In the analysis of line width data for the single and double mutants containing distal and proximal fluorine probes, it is important to select an appropriate ligation state as a standard for comparison of line width changes. As discussed below, comparison of proteins with different ligation states may result in spectral changes that are due to structural changes in the proteins. For example, comparison of deoxy Mb with MbNO results in differences in chemical shift values that are due, in part, to protein structural changes. To focus on the primary question of whether NO binds on the distal or proximal side in H93G-NO and to avoid complicating the line width analysis with possible structural changes, we chose to compare line width values for the single and double mutants within the same ligation state, using the single mutant data as a reference. We feel that spectra for the single mutant proteins serve as appropriate references because the diatomic ligand must bind on the distal side in the single mutant case in which the proximal His 93 residue is present.

Comparison of the proximal mutant NO complexes shows the chemical shifts and line widths to be fairly similar; the 5-coordinate L149C/H93G-NO signal broadening slightly by 6 Hz relative to the 6-coordinate complex. In contrast, the distal mutant NO complexes show the fluorine NMR peak to broaden by ∼80 Hz for the 5-coordinate S58C/H93G-NO relative to the 6-coordinate NO complex. The fluorine nucleus is characteristically quite sensitive to the presence of paramagnetic centers. This sensitivity manifests itself in the increased broadening of fluorine line widths with decreasing separation between the fluorine nucleus and a paramagnetic center (*18*, *19*, *29*, *30*). On the basis of estimates from wild-type and H93G Mb crystal structures, the fluorine labels were designed to be equidistant (∼15 Å) from the heme iron. A careful estimate of the distances between the heme iron and the fluorine probes is necessary for interpretation of the data. Two distances are relevant to this discussion: the physical distance between the heme iron and the CF_3 label, and the distance between the spin of the 5- or 6-coordinate FeNO complex and the CF_3 group.

Estimate of the Distance between CF_3 and Heme Fe. The distance between the cysteine thiol and fluorine atoms of trifluoroacetyl-labeled cysteine was calculated using MM2 and MOPAC energy minimization. MM2 calculations give S to F distances of 3.2, 4.5, and 4.5 Å, while MOPAC minimization gives 4.7, 4.5, and 5.2 Å for S to F distances.

Table 3: Estimates of the Distance between Fe and the TFA Label

	distance from Fe to Cys S (Å)[a]		distance from Fe to Lys N (Å)[b]	
protein	ave	range	ave	range
L149C	15.09	15.06−15.12	15.10	12.79−17.72
S58C	15.39	15.39	14.72	14.55−15.05
L149C/H93G	14.79	14.77−14.81	15.50	13.44−17.47
S58C/H93G	15.94	15.11−16.78	15.76	13.45−17.70

[a] Distances from Fe to the Cys thiol were estimated by substituting Cys at the appropriate mutation site in the PDB structure for each protein [i.e., 1IRC for H93G (*14*) and 1BZ6 for WT (*31*)], and measuring the distance between Fe and the cysteine thiol of the most favorable rotamer conformations. [b] Distances from Fe to the Lys N were estimated by substituting Lys at the appropriate mutation site in the PDB structure for each protein [i.e., 1IRC for H93G (*14*) and 1BZ6 for WT (*31*)], and measuring the distance between Fe and the lysine N of the most favorable rotamer conformations. Lys was chosen as a model of the TFA-labeled Cys side chain. The side chain N represents the terminal C of the TFA CF_3 group.

On average, the fluorine atoms are ∼4.5 Å from the cysteine thiol, leading to a zeroth order estimate of 15 ± 4.5 Å for the distance between the heme and the fluorine probes, based on wild-type and H93G(Im) crystal structure data. Further refinement of the estimate must incorporate the conformational constraints of the protein matrix. Using Swiss PBD Viewer software, the S58 and L149 residues were replaced with cysteine in the crystal structures of metH_2O H93G(Im) (1IRC) (*14*) and sperm whale WT (high resolution) (1BZ6) (*31*) to determine favorable side chain orientations in the protein context. Additionally, the S58 and L149 residues were replaced with lysine to mimic the TFA-labeled cysteine side chain, with the terminal NH_2 of Lys as a model for the CF_3 group. Values for the Fe to Cys thiol S and the Fe to Lys N distances are summarized in Table 3. Using the Lys NH_2 position gives an average distance from Fe to the CF_3 label that differs by 0.38 Å for the single mutants and 0.26 Å for the double mutants.

Localization of the NO• Spin. In ferrous MbNO samples, localization of the NO• spin changes the effective distance between the paramagnetic Fe(II)−NO center and the fluorine probe. Single-crystal EPR measurements of MbNO and ^{15}NO-^{57}Fe-enriched MbNO samples show significant hyperfine coupling of the heme iron with both the NO nitrogen and the proximal histidine nitrogen. The distribution of spin density has been shown to be ∼44% on Fe, ∼55% on N of NO, and ∼5% on N_ϵ of His93 (*32*). ESEEM and ENDOR studies have shown additional hyperfine coupling between the heme iron and the heme pyrrole nitrogens as well as N_ϵ of the distal histidine H64 via hydrogen bonding with NO. Coupling to the heme pyrrole nitrogens (∼3 MHz) and the distal histidine N_ϵ (∼5 MHz) are both much weaker than coupling to NO (∼40 MHz) or the proximal His N_ϵ (∼17 MHz) (*33*, *34*). EPR, ESEEM, and ENDOR results indicate that the NO spin couples to the iron of MbNO, with about half of the spin density residing on the N atom of NO. As a result, the effective distance between the Fe−NO spin and the CF_3 probe is shortened by ∼1.9 Å, the Fe−N bond length of NO bound to Mb (*22*).

The observed line broadening effect is much more pronounced for the 5-coordinate NO complexes than for the 6-coordinate complexes. It is possible that structural differences between the 5- and 6-coordinate MbNO complexes may contribute to this result. X-ray crystal structures of model NO-bound porphyrin compounds show that the iron is displaced by 0.26−0.36 Å from the porphyrin plane in 5-coordinate Fe−NO complexes, whereas the iron is displaced by only ∼0.07 Å from the porphyrin plane in 6-coordinate complexes (*35*, *36*). This difference in heme Fe doming would move the NO closer to the fluorine probe in the 5-coordinate H93G-NO complex relative to the 6-coordinate complex. If NO were bound on the distal side of the heme in H93G-NO, Fe doming would enhance broadening of the distal fluorine probe in 5-coordinate as compared with 6-coordinate MbNO. Although this explanation is consistent with line width observations for the S58C distal mutants, it does not account for the 6 Hz broader line width observed for 5-coordinate L149C/H93G-NO as compared with 6-coordinate L149C/H93G(Im)NO. Structural changes favoring the distal probe are not expected to cause broadening of the proximal fluorine probe as well.

Alternatively, the 5-coordinate MbNO results may be due to changes in the spin state of 5-coordinate MbNO relative to 6-coordinate MbNO. The increased line width of the 5-coordinate proximal double mutant suggests that the 5-coordinate Fe−NO complex may exhibit an electron spin density distribution that differs from that of the 6-coordinate MbNO complex. It is possible that the spin state either increases in magnitude or becomes a mixed spin system upon converting from the 6-coordinate to the 5-coordinate MbNO species. Previous EPR characterization of the 6-coordinate wild-type MbNO, H93G(Im)NO, and the 5-coordinate H93G-NO complexes indicates that both the 5- and 6-coordinate complexes of the H93G single mutant are low-spin paramagnetic centers, $S = 1/2$ at 77 K (*11*). The EPR signals of the 6-coordinate NO complexes are split by hyperfine coupling interactions with both nitric oxide and the pyrrole nitrogens of histidine or imidazole in wild-type MbNO and H93G(Im)NO, respectively (*11*). The observation of hyperfine coupling in the 6-coordinate EPR data suggests that the spin density is delocalized across the Im−Fe−NO bonds. Removal of the imidazole ligand to generate the 5-coordinate H93G-NO complex eliminates the hyperfine coupling with imidazole, thereby eliminating coupling of the Fe−NO spin with the proximal side of heme. As a result, the paramagnetic spin density is asymmetrically distributed, further offset from the heme plane in the direction of the NO ligand. This effect generates line width changes analogous to that of differential heme Fe doming in 5- and 6-coordinate MbNO, as described above. As with structural differences, changes in the distribution of the paramagnetic spin density does not account for broadening of the proximal F signal. It is possible that the low temperature EPR data collected at 77 K does not adequately represent the spin state of the 5- and 6-coordinate MbNO complexes at room temperature. The room temperature NMR spectra may reflect samples that contain a mixture of low and intermediate spin states. If the spin or magnetic susceptibility of the 5-coordinate Fe−NO complexes differs significantly from that of the 6-coordinate MbNO complexes, the interaction between the Fe−NO center and the fluorine probe may be perturbed, thereby altering the observed line broadening effect. Thus, the observed enhanced line broadening could arise from a combination of both structural and spin distribution differences between the 5- and 6-coordinate MbNO species.

The observation of a broader ^{19}F resonance for the S58C and S58C/H93G MbNO complexes relative to the L149C and L149C/H93G MbNO complexes leads to the conclusion that the fluorine label on the distal side of the protein is closer to the bound NO than the fluorine label attached to the proximal side. In short, the fluorine NMR data are consistent with NO binding on the distal side of heme in H93G. Subsequent work in our lab has confirmed the conclusion that NO is bound on the distal side of H93G in an independent experiment that uses the vibrational stretching frequency of bound NO in a series of distal and proximal side mutants as a probe for the NO location (*37*).

Effects of Ligation States on Fluorine NMR Spectra. Fluorine NMR spectra of deoxy, CO, NO, oxy, met H_2O, and met CN bound forms of the TFA-labeled cysteine Mb mutants are depicted in Figure 3. Chemical shift values and line widths for these spectra are listed in Tables 1 and 2. Chemical shift and line width values for each ligation state are quite similar for single mutants and their corresponding double mutants. Comparison of line width values for a given mutant in the deoxy, CO, oxy, met CN, and met H_2O bound forms gives differences between the proximal and distal mutants that are relatively small, ranging from 1 to 6 Hz. In many cases, the line width comparison across ligation states leads to differences that are not significant with respect to the observed experimental variation for the line width measurements as listed in Table 2. For example, comparing line widths for the paramagnetic 6-coordinate MbNO species relative to the diamagnetic MbCO species gives differences of 1 and 2 Hz for S58C and L149C, respectively, but 2 Hz for both S58C/H93G(Im) and L149C/H93G(Im). Unfortunately, such small changes in line width are too small to be significant in light of the observed experimental error. As indicated above, all comparison of line width changes were restricted to data for the same ligation state.

For a given mutant, chemical shift varies more closely with the heme ligand identity than with the oxidation state or spin state of the heme iron complex. Met CN bound samples exhibit chemical shift values that are very similar for all four mutants, with met CN peaks appearing farthest downfield in all cases. The met H_2O spectra depict two peaks that are attributed to a mixture of met H_2O and met OH^- species in the samples. In most cases, the met H_2O peak dominates the spectrum, as expected at pH 7. However, the peak attributed to met OH^- becomes more prominent in the L149C spectrum, where the single and double mutant spectra are quite different. Chemical shift values vary most between the deoxy, CO, NO, and oxy forms of different mutants. In each mutant, chemical shift values for the 6-coordinate NO and CO bound proteins are virtually identical. The observation that the chemical shifts for CO and 6-coordinate NO bound proteins are the same, even though MbCO is diamagnetic, and 6-coordinate MbNO is paramagnetic ($S = 1/2$), suggests that coordination geometry, not spin states, contributes to chemical shift values. Moreover, the spectral differences between deoxy and CO bound samples, both Fe(II) heme centers, suggest that oxidation states are not solely responsible for chemical shift variations in these mutants. Surprisingly, spectra for the oxy bound samples are very similar to the deoxy spectra rather than the CO or NO spectra, for a given mutant. However, oxy and deoxy spectra are quite different for the S58C mutants as compared to the L149C mutants. Nevertheless, the fluorine chemical shift values seem to be affected most by differences in the ligands that bind to the heme, rather than oxidation or spin states. In other words, changing the distal ligand identity, and thus the heme geometry, alters the myoglobin structure in a way that is translated to the location of the TFA label, thereby affecting the ^{19}F chemical shift. Similarly, Pearson and co-workers report observing changes in chemical shift values for 4-fluorotryptophan residues incorporated at positions 7 and 14 in sperm whale Mb (*38*). ^{19}F NMR spectra for CO, oxy, deoxy, met H_2O, and met CN forms of the 4-fluorotryptophan-modified Mb exhibit a range in chemical shift values of 0.4 and 0.8 ppm for probe resonances at positions 7 and 14, respectively. Spectral changes are attributed to structural effects of the various ligands, although the observed pattern of shifts differs from the pattern that we report in this paper. However, the effect of ligands on ^{19}F probe chemical shifts is expected to vary with the location of the probe in the protein (see below).

The fluorine probes introduced at engineered cysteine residues that are ~15 Å away from the heme iron are affected by changes in the heme iron geometry induced by heme ligands. Changes in the heme environment induced by ligation of CO or NO are translated from the local heme environment to the periphery of the protein most likely by concerted motion of Mb helices. The location of the fluorine-labeled cysteine residue determines the extent and direction of chemical shift effects. Fluorine chemical shifts are affected by degree of solvent exposure as well as interactions with neighboring groups (*19*). Changes in the conformation of the protein backbone can lead to changes in the orientation of amino acid side chains, especially in flexible regions of the protein. Changes in the orientation of neighboring amino acids would alter the degree of hydrogen bonding and van der Waals interactions between those residues and the fluorine probe, thereby leading to changes in fluorine chemical shift values. In the case of fluorine-labeled L149C mutants, changes in the heme geometry can be translated via the F-helix where the proximal histidine residue is located. F-helix residues directly interact with residues on the H-helix, such as L149C. Furthermore, changes in the H-helix orientation relative to the F-helix can lead to changes in the flexibility and degree of solvent exposure of the proximal fluorine probe. Analogously, changes in the heme environment can be translated to the E-helix through the distal histidine residue (His 64) that interacts directly with the ligand bound in the distal heme pocket. Movement of the E-helix propagates along its length to residue 58, located at the N-terminal end of the E-helix. As a result, changes in the heme ligand can cause changes in the position of the fluorine probe attached to the E-helix. As with the probe at L149C, changes in the orientation of the probe affect its interaction with neighboring residues, giving rise to changes in its chemical shift values. Thus, changes in the heme environment induced by the nature of the coordinating sixth ligand to the heme causes structural changes in the protein that are translated to the fluorine-labeled cysteine 15 Å away from the heme iron.

Changes in the protein geometry, not unlike what we describe here, have been observed in ultra high resolution X-ray crystal structures of sperm whale WT deoxy Mb and MbCO and have been proposed as a mechanism for CO

discrimination in Mb (and Hb) (*31*). Comparison of these structures shows differences in the relative positions of the E and F helices due to CO binding to the heme iron. The E and F helices rotate around a pivot point near Lys79, thereby displacing S58 and L149 residues. The C atom of S58 moves 0.22 Å closer to the heme iron, while the C atom of L149 moves 0.21 Å away from the heme iron upon CO binding to deoxy Mb. Although this motion is slight, it would be sufficient to affect interactions between residues in the region of S58 and L149 and may be sufficient to affect the fluorine chemical shifts in our TFA-labeled cysteine mutants. Moreover, ESR measurements of spin-labeled met H_2O and met CN Mb indicate that N-terminal residues, including residues of the E-helix, are susceptible to conformational changes induced by ligand binding, (i.e., CN binding to met Mb) (*39*). In contrast, these studies did not show an apparent effect of CN binding on C-terminal residues, a finding that conflicts with our own observations. Our ^{19}F NMR data illustrate the sensitivity of the periphery of the protein to concerted motions of the protein helices caused by changes in the heme ligation. The solution phase NMR results presented in this paper agree with the possibility of global changes in the Mb structure observed in high resolution X-ray crystal structure data that are potentially influenced by crystal packing effects.

If the fluorine probe were located at the protein surface in the plane of the heme, one would expect the effect of the heme ligation on fluorine chemical shift values to diminish. The ligation effects would be completely absent, provided that the probe were attached to a region of the protein backbone that does not move between the deoxy Mb and MbCO high-resolution structures. According to Bartunik et al., an ideal residue to select would be Lys79 because it lies very near the pivot point of the E and F helices and is not observed to move upon CO binding to deoxy Mb. Furthermore, Lys79 conveniently lies roughly in the plane of the heme. An interesting test of our hypothesis would be to generate the K79C variant, label the cysteine thiol, and compare ^{19}F NMR spectra for various ligation states of the TFA-labeled K79C variant, provided that this mutation does not disrupt the protein fold.

ACKNOWLEDGMENT

The strategy used in this paper resulted from discussions with Professor Gerd LaMar, and we are grateful for the stimulus.

SUPPORTING INFORMATION AVAILABLE

The UV/vis spectral peak positions of Soret and Q-bands for the cysteine mutants in the ligation states as described in the text (Table 1). The ^1H NMR spectral peak positions for the CN and CO bound cysteine mutants (Tables 2 and 3). ^1H and ^{19}F spectra for the glutathione (GSH), TFA-labeled glutathione (GSH-TFA), and dithionite-treated GSH-TFA control experiments (Figure 1). This material is available free of charge via the Internet at http://pubs.acs.org.

REFERENCES

1. Polizio, F., De Sanctis, G., Ascenzi, P., and Coletta, M. (1998) *J. Biol. Inorg. Chem. 3*, 458−462.
2. Ascenzi, P., Coletta, M., Desideri, A., and Brunori, M. (1985) *Biochim. Biophys. Acta 829*, 299−302.
3. Taketa, F., Antholine, W. E., and Chen, J. Y. (1978) *J. Biol. Chem. 253*, 5448−5451.
4. Henry, Y., and Banerjee, R. (1973) *J. Mol. Biol. 73*, 469−482.
5. Yonetani, T., Tsuneshige, A., Zhou, Y., and Chen, X. (1998) *J. Biol. Chem. 273*, 20323−20333.
6. Zhao, Y., Brandish, P. E., Ballou, D. P., and Marletta, M. A. (1999) *Proc. Natl. Acad. Sci. U.S.A. 96*, 14753−14758.
7. Stone, J. R., Sands, R. H., Dunham, W. R., and Marletta, M. A. (1995) *Biochem. Biophys. Res. Commun. 207*, 572−577.
8. Stone, J. R., and Marletta, M. A. (1994) *Biochemistry 33*, 5636−5640.
9. Yu, A. E., Hu, S., Spiro, T. G., and Burstyn, J. N. (1994) *J. Am. Chem. Soc. 116*, 4117−4118.
10. Barrick, D. (1994) *Biochemistry 33*, 6546−6554.
11. Decatur, S. M., Franzen, S., DePillis, G. D., Dyer, R. B., Woodruff, W. H., and Boxer, S. G. (1996) *Biochemistry 35*, 4939−4944.
12. Pond, A. E., Roach, M. P., Sono, M., Rux, A. H., Franzen, S., Hu, R., Thomas, M. R., Wilks, A., Dou, Y., Ikeda-Saito, M., Ortiz de Montellano, P. R., Woodruff, W. H., Boxer, S. G., and Dawson, J. H. (1999) *Biochemistry 38*, 7601−7608.
13. Roach, M. P., Pond, A. E., Thomas, M. R., Boxer, S. G., and Dawson, J. H. (1999) *J. Am. Chem. Soc. 121*, 12088−12093.
14. Barrick, D. (1995) *Curr. Opin. Biotechnol. 6*, 411−418.
15. Decatur, S. M., and Boxer, S. G. (1995) *Biochemistry 34*, 2122−2129.
16. Decatur, S. M., DePillis, G. D., and Boxer, S. G. (1996) *Biochemistry 35*, 3925−3932.
17. Danielson, M. A., and Falke, J. J. (1996) *Annu. Rev. Biophys. Biomol. Struct. 25*, 163−195.
18. Gerig, J. T. (1994) *Prog. Nucl. Magn. Reson. Spectrosc. 26*, 293−370.
19. Gregory, D. H., and Gerig, J. T. (1991) *Biopolymers 31*, 845−858.
20. Huestis, W. H., and Raftery, M. A. (1972) *Biochemistry 11*, 1648−1654.
21. Huestis, W. H., and Raftery, M. A. (1978) *Biochem. Biophys. Res. Commun. 81*, 892−899.
22. Brucker, E. A., Olson, J. S., Ikeda-Saito, M., and Phillips, G. N. (1998) *Proteins: Struct. Funct. Genet. 30*, 352−356.
23. DePillis, G. D., Decatur, S. M., Barrick, D., and Boxer, S. G. (1994) *J. Am. Chem. Soc. 116*, 6981−6982.
24. Ellman, G. L. (1959) *Arch. Biochem. Biophys. 82*, 70−77.
25. Emerson, S. D., and La Mar, G. N. (1990) *Biochemistry 29*, 1545−1556.
26. Mabbutt, B. C., and Wright, P. E. (1985) *Biochim. Biophys. Acta 832*, 175−185.
27. Dalvit, C., and Wright, P. E. (1987) *J. Mol. Biol. 194*, 313−327.
28. Brown, W. E., and Seamon, K. B. (1978) *Anal. Biochem. 87*, 211−222.
29. Gamcsik, M. P., Gerig, J. T., and Gregory, D. H. (1987) *Biochim. Biophys. Acta 912*, 303−316.
30. Arseniev, A. S., Utkin, Y. N., Pashkov, V. S., Tsetlin, V. I., Ivanov, V. T., Bystrov, V. F., and Ovchinnikov, Y. A. (1981) *FEBS Lett. 136*, 269−274.
31. Kachalova, G. S., Popov, A. N., and Bartunik, H. D. (1999) *Science 284*, 473−476.
32. Dickinson, L. C., and Chien, J. C. W. (1974) *Biochem. Biophys. Res. Commun. 59*, 1292−1297.
33. Tyryshkin, A. M., Dikanov, S. A., Reijerse, E. J., Burgard, C., and Hüttermann, J. (1999) *J. Am. Chem. Soc. 121*, 3396−3406.
34. Höhn, M., Hüttermann, J., Chien, J. C. W., and Dickinson, L. C. (1983) *J. Am. Chem. Soc. 105*, 109−115.
35. Scheidt, W. R., and Frisse, M. E. (1975) *J. Am. Chem. Soc. 97*, 17−21.
36. Scheidt, W. R., Duval, H. F., Neal, T. J., and Ellison, M. K. (2000) *J. Am. Chem. Soc. 122*, 4651−4659.
37. Thomas, M. R., and Boxer, S. G., unpublished results.
38. Pearson, J. G., Montez, B., Le, H., Oldfield, E., Chien, E. Y. T., and Sligar, S. G. (1997) *Biochemistry 36*, 3590−3599.
39. Postnikova, G. B. (1996) *Biochemistry (Moscow) 61*, 679−693.

BI0101087